Applied Physics Letters

RESEARCH ARTICLE | FEBRUARY 19 2013

Hydrogen plasma microlithography of graphene supported on a Si/SiO_2 substrate

Baran Eren; Thilo Glatzel; Marcin Kisiel; ... et. al

Appl. Phys. Lett. 102, 071602 (2013)
https://doi.org/10.1063/1.4793197

Hydrogen plasma microlithography of graphene supported on a Si/SiO_2 substrate

Baran Eren,[a] Thilo Glatzel, Marcin Kisiel, Wangyang Fu, Rémy Pawlak, Urs Gysin, Cornelia Nef, Laurent Marot, Michel Calame, Christian Schönenberger, and Ernst Meyer
Department of Physics, University of Basel, Klingelbergstrasse 82, CH-4056 Basel, Switzerland

(Received 3 December 2012; accepted 7 February 2013; published online 19 February 2013)

In this work, a silicon stencil mask with a periodic pattern is used for hydrogen plasma microlithography of single layer graphene supported on a Si/SiO_2 substrate. Obtained patterns are imaged with Raman microscopy and Kelvin probe force microscopy, thanks to the changes in the vibrational modes and the contact potential difference (CPD) of graphene after treatment. A decrease of 60 meV in CPD as well as a significant change of the D/G ratio in the Raman spectra can be associated with a local hydrogenation of graphene, while the topography remains invariant to the plasma exposure. © *2013 American Institute of Physics*. [http://dx.doi.org/10.1063/1.4793197]

In the last decades, the interaction of hydrogen with graphitic surfaces has been investigated various times. The earlier research was focused on the physisorption of hydrogen molecules on such surfaces.[1–3] This was followed by studies which were concentrated on the chemisorption of atomic hydrogen.[4–9] A more recent research focus involves plasma treatment of such surfaces with plasmas containing hydrogen.[10,11] For instance, Elias *et al.* had evidences of graphane growth (full hydrogenation of graphene from both sides) after exposure of free-standing graphene to a plasma containing 10% of hydrogen.[10] Previously, we have characterized hydrogen plasma treated graphite using various methods.[12]

In this work, we used a silicon stencil mask with a periodic hole structure in order to pattern altered and pristine graphene, which was grown by chemical vapor deposition (CVD) and transferred onto a Si/SiO_2 (p-doped Si, SiO_2 thickness is 86 nm) wafer. Raman microscopy and Kelvin probe force microscopy (KPFM) were used to image these patterns, indicating the changes in the vibrational modes and the contact potential difference (CPD) after hydrogen plasma treatment.

Single layer graphene was grown on a copper foil in a split quartz tube furnace using a CVD method involving methane and hydrogen gases.[13] Transfer of the graphene layer onto the Si/SiO_2 substrate was achieved by the standard procedure involving PMMA coating, dissolving the copper foil in an iron nitrate solution, "fishing" the polymer with the substrate, and the removal of PMMA in acetone.[13] The obtained graphene layers (with a size of more than 1 cm^2) showed a very weak response to pH changes, manifesting their quality thanks to the scarcity of defect-induced dangling bonds.[14] The hydrogen plasma treatment was performed in a specially designed radio frequency (RF) plasma exposure facility.[15] The hydrogen gas pressure was fixed to 3 Pa, where the background pressure was 5×10^{-6} Pa. Plasma was created ~75 cm away from the sample in a Pyrex tube through a matching network by a 13.56 MHz RF generator at a typical power of 49 W. This RF power was coupled to the tube by an outer electrode (surfatron).[16] The used hydrogen plasma had an electron temperature of 3.5 ± 0.5 eV and an ion flux of $1.5 \pm 0.5 \times 10^{15}\,cm^{-2}s^{-1}$. The sample was kept electrically floating during 5 min of exposure. With this technique, proton deposition energies can be obtained which are high enough to overcome the energy barrier (3.7 eV) to penetrate the center of the hexagonal carbon,[17] without physically sputtering (36 eV) the carbon atoms.[18] More detailed information about the plasma can be found in Ref. 12.

Raman microscopy measurements were performed using a WITec alpha 300 confocal Raman microscope. The wavelength of the excitation laser was 532 nm and the power of the laser was kept at 2.1 mW without noticeable sample heating or damaging. The laser spot size was 360 nm at 100× magnification. The spectral resolution was 3 cm^{-1}. The Raman spectrum of graphene consists of the D and G peaks,[19–22] around 1345 cm^{-1} and 1590 cm^{-1}, respectively, which arise from vibrations of sp^2-hybridized carbon atoms (Figure 1(a)—black line). The cross-section for the C-C sp^3 vibrations, when available, is negligible for visible excitation. The G peak represents the optical E_{2g} phonons at the center of the Brillouin zone. The D peak is caused by breathing-like modes corresponding to transverse optical phonons near the K point of the Brillouin zone. It is an intervalley double-resonance Raman processes which is initiated only by a deviation from the defectless two dimensional character.[19,20,22] Its overtone, the 2D peak which appears around 2685 cm^{-1}, is a second order process involving two inelastic scatterings and is always present.

Upon hydrogen plasma exposure, a sharp D' peak around 1625 cm^{-1} appears as a result of intervalley double-resonance process due to deviation from the defectless two dimensional character as well as an increase in the D peak intensity (Figure 1(a)—red line). A negative shift can be observed at the 2D peak position after plasma treatment. This shift suggests an increase in the electron concentration (i.e., an upper shift of the Fermi level),[23] suggesting electron donation from chemically bound hydrogen atoms. On the contrary to this point, the G peak preserves its position at 1590 cm^{-1}. The sharpness of the peaks signifies that amorphization is negligible.[20]

[a]Electronic mail: baran.eren@unibas.ch.

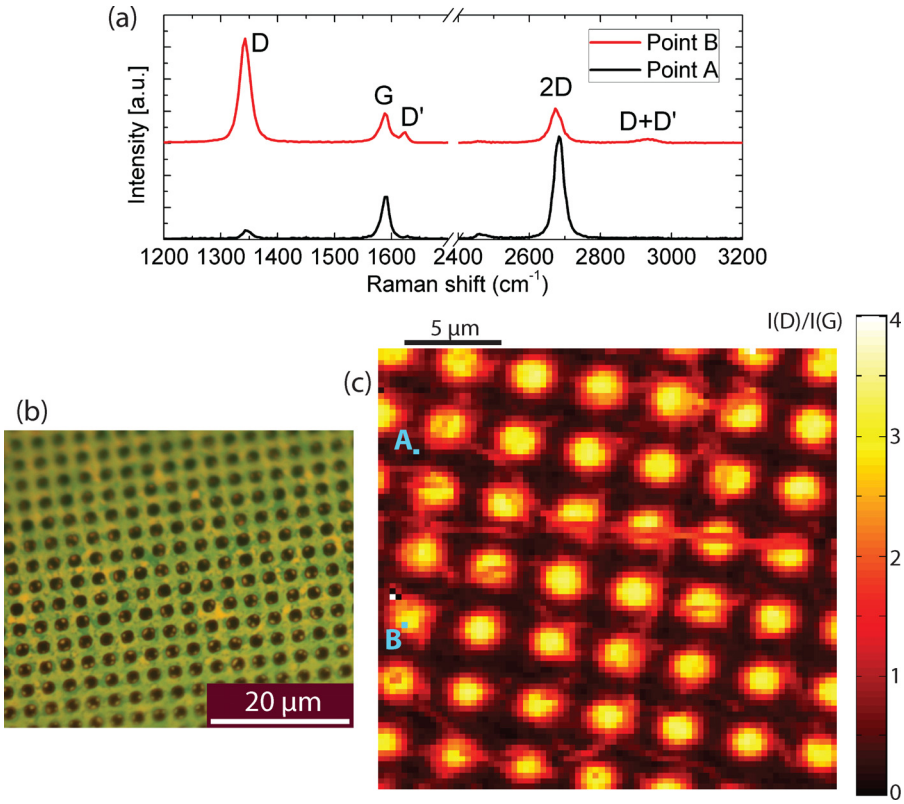

FIG. 1. (a) Typical Raman spectra of covered (black) and plasma treated (red) parts of graphene supported on Si/SiO_2. (b) Optical microscope image of the silicon stencil mask used for plasma microlithography. (c) $20 \times 20\,\mu m^2$ (80×80 pixels) Raman microscopy of patterned graphene, showing a clear increase of the D peak to G peak intensity ratio at the plasma treated areas.

Due to the above mentioned differences of the Raman spectrum before and after exposure, monitoring the intensity ratio of D peak to G peak is an adequate solution for imaging the exposure patterns. A $20 \times 20\,\mu m^2$ image was obtained by scanning the x-y stage with steps of 250 nm. An integration time of 1 s was used for each pixel. The Raman microscopy image showing the intensity ratio I(D)/I(G) (Figure 1(c)) of the hydrogen plasma exposed single layer graphene reveals the general shape of the patterns of the stencil mask (Figure 1(b)). A clear increase of this ratio of up to 4 was observed at the plasma treated areas, proving that the hydrogen plasma microlithography of graphene can be applied. This ratio was also obtained in various works involving hydrogen plasma and was correlated with hydrogenation of graphene.[10,24,25]

To address the question of the origin and the properties of the treated areas, KPFM was applied which provides a combined information on the topography and the surface potential. A strong topographic corrugation related to plasma induced defects might be the origin of the increase in the D peak intensity. However, for a local hydrogenation of graphene, a change of the work function in such areas is expected and can be measured by variations of CPD.[26]

Figure 2 shows topography and CPD images of the untreated graphene layer transferred onto Si/SiO_2 substrate measured by KPFM using a Nanosurf FlexAFM operated in ambient conditions in a controlled dry nitrogen atmosphere in a glove box. The scan range of the measurement was $10 \times 10\,\mu m^2$. A commercially available Nanosensors PPP-EFM silicon cantilever with a platinum/iridium (Pt/Ir) coating was used. The fundamental cantilever resonance frequency ($f_{1^{st}} \sim 62$ kHz) was excited to obtain topographical information, whereas the second flexural cantilever resonance ($f_{2nd} \sim 400$ kHz) was used for the CPD detection in the intermittent contact regime.[27,28] While the AC voltage exciting the electrostatic force modulation was applied to the sample, the DC voltage was applied to the tip. The CPD data are represented in such a way that the bright areas correspond to areas with a larger work function values.

The measurements can be used for the estimation of the absolute work function. Under the assumption that the AFM tip remained unchanged before acquisition of Figure 2, Pt/Ir coated tips used in this work have a work function of 4.28 eV,[29] revealing a work function of around 4.75 eV for the as prepared single layer graphene on Si/SiO_2. Of course, this value may not be accurate and it can vary 100 s of meV depending on the conditions of the tip; however, the precision of the CPD variation is in the order of 10 meV. The work function of graphene supported on a Si/SiO_2 substrate, in the simplest picture, is the sum of the work function of free-standing graphene (4.23 eV (Refs. 30 and 31)) and the energy gain due to the surface charge density. This surface charge density is induced by electrostatic charging and charge rearrangements in the proximity of SiO_2, including the effects from the interface contaminants. This, in a way, can be interpreted as p-type doping of graphene,[32] as it is donating electrons into SiO_2 and/or to the contaminants at the interface. This process results in a downward shift of the Fermi level, hence an increase in the work function of graphene.[30] Using the equation given in Ref. 30, it can be very roughly estimated that graphene is doped with 2×10^{13} holes/cm^2 for a Fermi velocity of 10^6 m/s. A recent KPFM measurement of the work function of graphene on 300 nm SiO_2 was reported to be 4.57 eV.[33] However, a recent study predicts rather an n-type behavior of graphene supported on Si/SiO_2, after removal of adsorbed gases in ultra-high vacuum (UHV).[31] In this respect, it can be anticipated that the

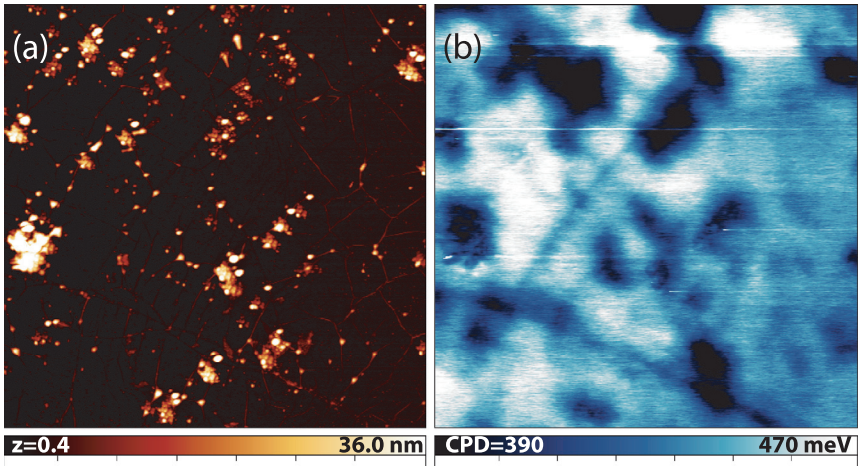

FIG. 2. $10 \times 10\,\mu m^2$ (a) topography and (b) CPD images of the pristine graphene layer supported on a Si/SiO_2 substrate, measured in a dry nitrogen atmosphere.

hole doping originates from the surface/interface contaminants, e.g., water.

The pristine graphene films show some microscopic ripples and round-like protrusions with heights of up to 50 nm (Figure 2(a)). The ripples are due to the stress in the graphene film, generated during cool-down after CVD growth as well as imperfections during transfer onto the Si/SiO_2 substrate. Two of the ripples can also be observed in the same image with lower CPD values (Figure 2(b)). The ripples do not have contact with SiO_2, which results in a weaker electrostatic charging of graphene and therefore, they are observed as zones with a lower work function. Alternatively, these two ripples might also be grain boundaries of graphene, which are, in fact, bilayer graphene because of the overlap of two graphene layers. Similarly, in the Raman map presented in Figure 1(c), some ripple-like features are also present due to the increase in the D peak intensity. The round-like protrusions are left overs of the PMMA polymer during the transfer onto SiO_2, resulting in a reduced CPD of up to 80 meV.

Figure 3 shows the topography and CPD images of masked graphene after plasma exposure. The topography image shows no structural effects created by the plasma exposure, whereas the CPD image clearly reflects the patterns of the stencil mask used. This result shows the strength of KPFM by resolving local work function variations, which appear solely due to chemical modifications of the surface, without any topographical contribution. The exposed areas exhibit patterns with reduced CPD of 60 ± 20 meV (Figures 3(b)–3(d)), indicating a lower work function for the hydrogen plasma treated areas. A small averaging effect might even further increase the variation of CPD by several 10 s of meV.[34]

Finally, in order to address the effects of the surface and interface contaminants, the KPFM measurements were repeated in UHV conditions using a home-built AFM operated in constant height mode and a Nanonis control unit. Though the absolute work function of graphene on SiO_2 decreased gradually during storage in UHV, the relative

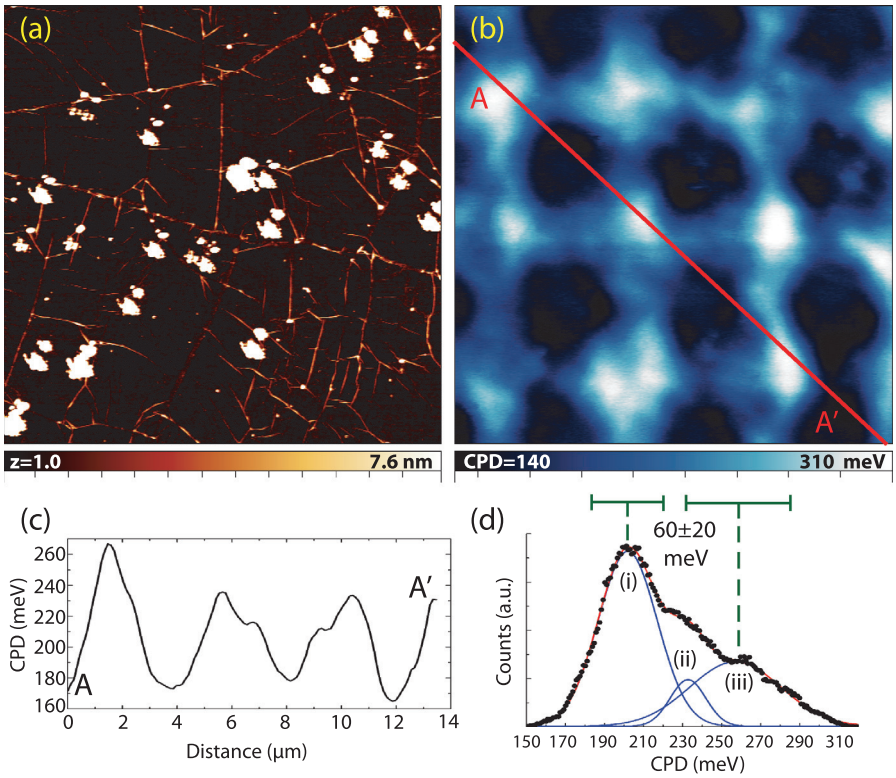

FIG. 3. $10 \times 10\,\mu m^2$ (a) topography and (b) CPD images of CVD grown graphene patterned with hydrogen plasma microlithography. Darker CPD contrasts are the plasma exposed areas. (c) CPD profile of the A-A′ line in (b). The histogram of (b) is shown in (d), in which the three Gaussian peaks correspond to 3 different contrasts of the CPD image. The difference between peaks (i) and (iii) which correspond to the dark and bright areas is 60 ± 20 meV. Peak (ii) is due to the averaging effects and corresponds to the areas in between dark and bright areas.

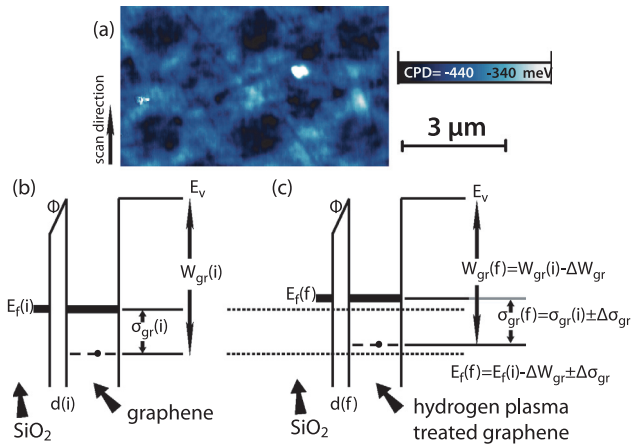

FIG. 4. (a) CPD image of patterned graphene after annealing at 130 °C in UHV. Potential diagram of graphene supported on clean Si/SiO_2 before (b) and after (c) hydrogen plasma treatment. W_{gr} denotes the work function of a free standing graphene. ϕ is the potential drop across the graphene SiO_2 interface. E_v and E_f are the vacuum level and the Fermi level, respectively. σ_{gr} is the energy loss to the surface charge density of graphene created as a result of electrostatic charging at equilibrium distance d with respect to the substrate subscripts i and f denote the pristine and hydrogen plasma treated graphene, respectively.

CPD contrast between the hydrogen plasma treated and untreated areas remained unchanged. Furthermore, in order to degas/desorb the contaminants out from the interface more efficiently, the sample was annealed at 130 °C for 1 h. Figure 4(a) shows the KPFM image, where the absolute work function graphene on SiO_2 can be estimated as ~3.9 eV, with a reduction of ~60 meV for the hydrogen plasma treated zones. This result confirms the predictions that single layer graphene should have a net electron transfer from SiO_2 in the absence of any interface impurities.[31,35]

Figure 4(b) shows a model of a potential diagram of graphene on clean SiO_2. In this picture, the work function of graphene supported on a Si/SiO_2 substrate is the sum of work function of a free standing graphene (W_{gr}) and the change in the surface potential ($-\sigma_{gr}$) in the proximity of SiO_2: $E_v - E_f(i) = 3.9\,\text{eV} = W_{gr} - \sigma_{gr}$. Figure 4(c) represents the potential diagram where the effects of hydrogen plasma treatment of graphene are addressed. As free-standing graphene starts to be decorated with hydrogen atoms from both sides, there is an upward shift of its Fermi level,[26] which is represented as ΔW_{gr} in our model. This can be understood in terms of electronegativity, where less electronegative hydrogen atoms behave like electron donors. In addition to this, hydrogenated graphene would also experience different electrostatic charging from the SiO_2 support, represented as $\Delta\sigma_{gr}$. With respect to the last point, variation in the measured CPD reflects the change of the work function of graphene with a modulation related to the difference in electrostatic charging: $\Delta CPD = 60 \pm 20\,\text{meV} \leq E_f(i) - E_f(f) = \Delta W_{gr} \pm \Delta\sigma_{gr}$.

In summary, we have employed hydrogen plasma microlithography on single layer graphene. The obtained results can pave the way to nanolithography of graphene prepared by hard mask techniques. We have utilized Raman and Kelvin probe force microscopy techniques for imaging the lithography pattern of graphene. Moreover, we have measured an absolute work function of around 3.9 eV for single layer graphene supported on a Si/SiO_2 substrate, whereas this value is 4.75 eV for as prepared single layer graphene on Si/SiO_2 due to hole doping from the surface interface contaminants. Finally, we have shown that the hydrogen plasma treatment of graphene on SiO_2 results in a work function reduction around 60 ± 20 meV and is explained by hydrogenation of the graphene layer. This may be an important step forward for the comprehension of the properties of hydrogenated graphene.

The authors would like to thank the Swiss Federal Office of Energy and the Federal Office for Education and Science for their financial support. This work was also supported by the Swiss National Foundation (SNF) and the National Centre of Competence in Research on Nanoscale Science (NCCR Nano).

[1]A. C. Dillon, K. M. Jones, T. A. Bekkedahl, C. H. Kiang, D. S. Bethune, and M. J. Heben, Nature **386**, 377 (1997).
[2]A. Züttel, P. Sudane, P. Maurona, T. Kiyobayashib, C. Emmeneggera, and L. Schlapbach, Int. J. Hydrogen Energy **27**, 203 (2002).
[3]F. L. Darkrim, P. Malbrunot, and G. P. Tartaglia, Int. J. Hydrogen Energy **27**, 193 (2002).
[4]T. Yildirim, O. Gulseren, and S. Ciraci, Phys. Rev. B **64**, 075404 (2001).
[5]B. N. Khare, M. Meyappan, A. M. Cassell, C. V. Nguyen, and J. Han, Nano Lett. **2**, 73 (2002).
[6]P. Ruffieux, O. Gröning, M. Bielmann, P. Mauron, L. Schlapbach, and P. Gröning, Phys. Rev. B **66**, 245416 (2002).
[7]D. Neumann, G. Meister, U. Kürpick, A. Goldmann, J. Roth, and V. Dose, App. Phys. A **55**, 489 (1992).
[8]A. Nikitin, H. Ogasawara, D. Mann, R. Denecke, Z. Zhang, H. Dai, K. Cho, and A. Nilsson, Phys. Rev. Lett. **95**, 225507 (2005).
[9]L. Hornekær, Ž. Šljivančanin, W. Xu, R. Otero, E. Rauls, I. Stensgaard, E. Lægsgaard, B. Hammer, and F. Besenbacher, Phys. Rev. Lett. **96**, 156104 (2006).
[10]D. C. Elias, R. R. Nair, T. M. G. Mohiuddin, S. V. Morozov, P. Blake, M. P. Halsall, A. C. Ferrari, D. W. Boukhvalov, M. I. Katsnelson, A. K. Geim, and K. S. Novoselov, Science **323**, 610 (2009).
[11]M. Wojtaszek, N. Tombros, A. Caretta, P. H. M. van Loosdrecht, and B. J. van Wees, J. Appl. Phys. **110**, 063715 (2011).
[12]B. Eren, D. Hug, L. Marot, R. Pawlak, M. Kisiel, R. Steiner, D. M. Zumbühl, and E. Meyer, Beilstein J. Nanotechnol. **3**, 852 (2012).
[13]X. Li, W. Cai, J. An, S. Kim, J. Nah, D. Yang, R. Piner, A. Velamakanni, I. Jung, E. Tutuc, S. K. Banerjee, L. Colombo, and R. S. Ruoff, Science **324**, 1312 (2009).
[14]W. Fu, C. Nef, O. Knopfmacher, A. Tasarov, M. Weiss, M. Calame, and C. Schönenberger, Nano Lett. **11**, 3597 (2011).
[15]M. Wisse, B. Eren, L. Marot, R. Steiner, and E. Meyer, Rev. Sci. Instrum. **83**, 013509 (2012).
[16]B. Eren, L. Marot, M. Langer, R. Steiner, M. Wisse, D. Mathys, and E. Meyer, Nucl. Fusion **51**, 103025 (2011).
[17]Y. G. Zhou, X. T. Zu, F. Gao, J. L. Nie, and H. Y. Xiao, J. Appl. Phys **105**, 014309 (2009).
[18]J. Bohdansky, J. Roth, and H. L. Bay, J. Appl. Phys **51**, 2861 (1980).
[19]F. Tuinstra and J. L. Koenig, J. Chem. Phys. **53**, 1126 (1970).
[20]A. C. Ferrari and J. Robertson, Phys. Rev. B **61**, 14095 (2000).
[21]A. C. Ferrari, J. C. Meyer, V. Scardaci, C. Casiraghi, M. Lazzeri, F. Mauri, S. Piscanec, D. Jiang, K. S. Novoselov, S. Roth, and A. K. Geim, Phys. Rev. Lett. **97**, 187401 (2006).
[22]A. C. Ferrari, Solid State Commun. **143**, 47 (2007).
[23]A. Das, S. Pisana, B. Chakraborty, S. Piscanec, S. K. Saha, U. V. Waghmare, K. S. Novoselov, H. R. Krishnamurthy, A. K. Geim, A. C. Ferrari, and A. K. Sood, Nat. Nanotechnol. **3**, 210 (2008).
[24]Y. Wang, X. Xu, J. Lu, M. Lin, Q. Bao, B. Özyilmaz, and K. P. Loh, ACS Nano **4**, 6146 (2010).
[25]Z. Luo, T. Yu, Z. Ni, S. Lim, H. Hu, J. Shang, L. Liu, Z. Shen, and J. Lin, J. Phys. Chem. C **115**, 1422 (2011).
[26]X. Peng, F. Tang, and A. Copple, J. Phys.: Condens. Matter **24**, 075501 (2012).
[27]A. Kikukawa, S. Hosaka, and R. Imura, Rev. Sci. Instrum. **67**, 1463 (1996).

[28]C. Sommerhalter, T. W. Matthes, T. Glatzel, A. Jäger-Waldau, and M. C. Lux-Steiner, Appl. Phys. Lett. **75**, 286 (1999).
[29]S. Sadewasser, T. Glatzel, M. Rusu, A. Jäger-Waldau, and M. C. Lux-Steiner, Appl. Phys. Lett. **80**, 2979 (2002).
[30]D. Ziegler, P. Gava, J. Guttinger, F. Molitor, L. Wirtz, M. Lazzeri, A. M. Saitta, A. Stemmer, F. Mauri, and C. Stampfer, Phys. Rev. B **83**, 235434 (2011).
[31]H. E. Romero, N. Shen, P. Joshi, H. R. Gutierrez, S. A. Tadigadapa, J. O. Sofo, and P. C. Eklund, ACS Nano **2**, 2037 (2008).
[32]K. S. Novoselov, A. K. Geim, S. V. Morozov, D. Jiang, Y. Zhang, S. Dubonos, I. V. Grigorieva, and A. A. Firsov, Science **306**, 666 (2004).
[33]Y.-J. Yu, Y. Zhao, S. Ryu, L. E. Brus, K. S. Kim, and P. Kim, Nano Lett. **9**, 3430 (2009).
[34]G. Elias, T. Glatzel, E. Meyer, A. S. amd A. Boag, and Y. Rosenwaks, Beilstein J. Nanotechnol. **2**, 252 (2011).
[35]R. H. Miwa, T. M. Schmidt, W. L. Scopel, and A. Fazzio, Appl. Phys. Lett. **99**, 163108 (2011).